Reac Kinet Mech Cat (2017) 120:149–165
DOI 10.1007/s11144-016-1079-5

Reaction characteristics of KOH-modified copper manganese oxides catalysts for low-temperature CO oxidation in the presence of CO_2

Yafei Guo[1] · Shouxiang Lu[1] · Jin Lin[1] · Chuanwen Zhao[2] · Changhai Li[1]

Received: 14 June 2016 / Accepted: 31 August 2016 / Published online: 7 September 2016

Abstract Binary copper manganese oxides catalysts supported on different activated carbons were prepared using the co-precipitation and high-pressure impregnation methods. The catalysts were further modified by KOH to mitigate the adverse effect of CO_2 on their CO oxidation performances. The as-synthesized catalysts were characterized by N_2 adsorption–desorption, X-ray diffraction, field emission scanning electron microscopy, and Fourier transform infrared spectroscopy. The effects of support and synthesis method, CO concentration, CO_2 concentration, gas hourly space velocity (GHSV), and particle size on CO oxidation performances of the catalysts were investigated. The nature of the different activated carbon supports showed no significant effect on their CO oxidation performances. By contrast, the high-pressure impregnation method was conducive to more effective loading and uniform dispersion of the active components on the support and therefore to benefit the catalyst enhanced CO oxidation performances. Under the given experimental conditions, CO oxidation conversion decreased with the increase of CO concentration, CO_2 concentration, GHSV, and particle diameter.

Keywords Copper manganese oxides compound · KOH modification · CO oxidation · Catalyst deactivation · Reaction characteristics

Electronic supplementary material The online version of this article (doi:10.1007/s11144-016-1079-5) contains supplementary material, which is available to authorized users.

✉ Shouxiang Lu
sxlu@ustc.edu.cn

[1] State Key Laboratory of Fire Science, University of Science and Technology of China, Hefei 230026, Anhui, China

[2] Jiangsu Provincial Key Laboratory of Materials Cycling and Pollution Control, School of Energy and Mechanical Engineering, Nanjing Normal University, Nanjing 210042, Jiangsu, China

Introduction

Hazardous gases in post-fire smoke pose great threat to human safety and task performances in typical environmental control and life support systems (ECLSS) such as spacecrafts, submarines, and naval ship compartments. By far, poisoning induced by the high-concentration CO is considered as the prime reason for life casualties in fire [1–3]. Binary copper manganese oxides composites have been extensively utilized for catalytic removal of CO from ECLSS [4–8].

Recently, copper manganese oxides catalysts have been reported to exhibit good activity for CO oxidation at ambient temperature [9–24]. The catalysts might show promise for removing CO from post-fire smoke, and this has not been extensively reported. One significant concern of using copper manganese oxides catalysts for CO depollution treatment from post-fire smoke is that their CO oxidation activities might be adversely affected by the high concentration CO_2. There are some previous contributions highlighting the deactivation process of CO catalysts in the presence of CO_2. Hoflund et al. reported that Au exhibited decreased CO oxidation activities when exposed in the atmosphere containing CO_2 [25]. Liang et al. also found that CO_2 had an adverse effect on the stability of Pd/CeO_2-TiO_2 [26]. Parinyaswan et al. reported that CO_2 molecules could occupy the adsorption active sites over Pt–Pd/CeO_2. The catalyst deactivation process was deduced as the fact that the migration of mobile oxygen in the redox process had been inhibited by CO_2 molecules [27]. Furthermore, in the work of Wang et al., the inhibiting effect of CO_2 on the activity of Pd–Cu catalyst was attributed to several reasons as the competitive adsorption between CO and CO_2, the occlusion of adsorption active sites and the impediment effect on the transformation of intermediates [28]. Although catalyst deactivation for CO oxidation in the presence of CO_2 has received much attention, more efforts on improving the CO oxidation performances and mitigating the catalyst deactivation in the presence of CO_2 are necessary.

For supported catalysts, supporting materials with porous structures and basic/acid surface would affect their catalytic performances [29, 30]. Generally, surfaces, grooves, pores, and channels could be present in supporting materials, as shown in Fig. S1. The textural properties of the supports play significant roles in their CO oxidation performances. A large surface area and benign surface chemistry provide more active sites for adsorption. The dispersion state of active components over the surface of the supports also affect their CO oxidation behaviors. Grooves, pores, and channels play significant roles in that they provide space to accommodate more active components and offer contact zone for gas diffusion. Nevertheless, excessive loading of active components is expected to cause pore blockage and the covering of active sites, which are not conducive to enhanced CO oxidation performances. Moreover, the catalyst synthesis method influences the loading and dispersion of active components and therefore affect their CO oxidation performance. Furthermore, operating parameters such as CO concentration, CO_2 concentration, gas hourly space velocity (GHSV) and particle size could also be important factors affecting their CO oxidation activities. Hence, the effects of supporting material,

synthesis method and operating parameters on CO oxidation performances of the catalysts deserve more understanding.

In this work, copper manganese oxides precursors with different activated carbon supports are synthesized using the co-precipitation and high-pressure impregnation methods. The precursors are further modified by KOH to obtain the bi-functional catalysts with improved CO_2-resistance. The first objective is to evaluate the CO oxidation performances of the catalysts in the presence of CO_2. The effects of supporting material and synthesis method on CO oxidation performances are expounded, and the optimal candidate with high activity and excellent long-term working stability is screened. Furthermore, the effects of CO concentration, CO_2 concentration, GHSV, and particle size on CO oxidation performances are demonstrated.

Experimental

Materials

Coconut-shell activated carbon, coal activated carbon and wood activated carbon with an average particle diameter of 300 μm were selected as the supporting materials. They were purchased from Shandong Yimei Machinery Equipment Manufacturing Co., Ltd., Weihai Mingxiang Medical Devices Co., Ltd., and Jining Luyi Material Co., Ltd. Copper acetate ($C_4H_6CuO_4{\cdot}H_2O$, AR 99 %), manganese acetate ($C_4H_6MnO_4{\cdot}4H_2O$, AR 99 %), and potassium hydroxide (KOH, AR 99 %) were determined as the active components. They were provided by Tianjin Damao Chemical Reagent Factory, Tianjin Guangfu Fine Chemical Research Institute, and Shanghai Jiuyi Chemical Reagent Co., Ltd.

Catalyst synthesis

Synthesis of copper manganese oxides precursors

Copper manganese oxides precursors with different supports were synthesized by the co-precipitation and high-pressure impregnation methods. To facilitate description, the as-synthesized precursors were labeled as CM-P-CSAC, CM-P-CAC, CM-P-WAC, and CM-I-WAC. CM denoted copper manganese oxide compounds, P and I denoted the co-precipitation and high-pressure impregnation methods. CSAC, CAC, and WAC denoted the coconut-shell activated carbon, coal activated carbon and wood activated carbon.

CM-P-CSAC, CM-P-CAC, and CM-P-WAC were synthesized with the co-precipitation method. 10 g of KOH was first dissolved in 100 mL of deionized water under stirring to form KOH solution. 50 g of the supports (CSAC, CAC, and WAC) were mixed with certain grams of $C_4H_6CuO_4{\cdot}H_2O$ and $C_4H_6MnO_4{\cdot}4H_2O$ dissolved in 200 mL of deionized water under stirring at ambient temperature for 2 h. Then, KOH solution was added drop wise into the mixture under stirring for 4 h. The precipitates were then filtered and washed several times by deionized water

followed by drying in a rotary vacuum evaporator at 85 °C overnight and calcination in a muffle furnace at 350 °C for 6 h to obtain the desired precursors.

CM-I-WAC was synthesized with the high-pressure impregnation method. 50 g of the support (WAC) was mixed with certain grams of $C_4H_6CuO_4{\cdot}H_2O$ and $C_4H_6MnO_4{\cdot}4H_2O$ dissolved in 200 mL of deionized water under stirring overnight in a high-pressure vessel. The mixtures were then dried in a rotary vacuum evaporator at 85 °C overnight followed by calcination in a muffle furnace at 350 °C for 6 h to obtain the desired precursor.

Synthesis of the bi-functional catalysts

The bi-functional catalysts of KCM-P-CSAC, KCM-P-CAC, KCM-P-WAC, and KCM-I-WAC were prepared with the impregnation of KOH on the as-synthesized precursors. A certain gram of the precursors were mixed with 25 g of KOH dissolved in 250 mL of de-ionized water under stirring overnight at ambient temperature. The mixtures were subsequently dried in a rotary vacuum evaporator at 85 °C overnight and calcined in a muffle furnace at 350 °C for 6 h to obtain the desired bi-functional catalysts.

Catalyst characterization

X-ray diffraction (XRD) patterns of the catalysts were recorded on an X'Pert PRO diffractometer (Philips, Netherlands) using nickel-filtered Cu Kα radiation at 30 kV and 150 mA (2θ angle ranging from 10° to 70°, wavelength $\lambda = 0.15406$ nm and 0.02° sampling width). Texture parameters including the BET surface areas, pore volumes, and average pore diameters were determined from N_2 adsorption–desorption tests performed on an automatic surface area and porosity analyzer Tristar II 3020 M (Micromeritics, USA). Particle morphologies of the catalysts were observed by field emission scanning electron microscopy (FESEM) SIRION200 (Philips, Netherlands). Chemical compositions of the catalysts were determined by inductively coupled plasma-mass spectrometry (ICP-MS) X Series 2 (Thermo Fisher Scientific, USA).

Catalytic testing

CO oxidation tests were performed in a fixed-bed reactor with an inner diameter of 0.02 m and a height of 0.2 m. 5 g of the catalysts were packed in the reactor. Prior to each test, the reactor was heated to 200 °C in a pure N_2 stream to eliminate the adsorbed water vapor. Then, the reactor was cooled to ambient temperature. Gaseous mixtures of 0.4 %CO + 1 %CO_2 and balanced air with a total flow rate of 500 mL/min (GHSV = 4000 h^{-1}) then flowed through the reactor. The reactor was subsequently heated to the desired temperature with a ramping rate of 10 °C/min for CO oxidation test. By measuring the change of CO concentration at the outlet of the reactor with a gas analyzer, CO oxidation performances of these catalysts could be evaluated. By changing the operating parameters, the effects of CO concentration,

CO_2 concentration, GHSV, and particle size on CO oxidation performances could also be evaluated.

Catalytic activity evaluation

The as-synthesized catalysts were screened on the basis of their CO oxidation activities and long-term working stabilities. The CO conversion could be expressed as:

$$X = \frac{Q_{in}C_{CO}^{0} - Q_{out}C_{CO}^{f}}{Q_{in}C_{CO}^{0}} \times 100\ \% \quad (1)$$

Here X is the CO conversion, C_{CO}^{0} and C_{CO}^{f} are the CO concentrations at the inlet and outlet of the reactor. Q_{in} and Q_{out} are the total flow rates at the inlet and outlet of the reactor. Besides, the temperatures for half and total CO conversions (T_{50} and T_{100}) were recorded to evaluate their CO oxidation activities. Long-term working stabilities were characterized by the durations for keeping their stable CO conversions.

Results and discussion

Catalyst characterization

Chemical compositions

The chemical compositions of KCM-P-CSAC, KCM-P-CAC, KCM-P-WAC, and KCM-I-WAC were measured by ICP-MS, and the results are shown in Table 1. The contents of Cu and Mn species in KCM-I-WAC synthesized by the high-pressure impregnation method are high as 13.20 and 30.80 wt%. By contrast, the contents of Cu and Mn in KCM-P-CSAC, KCM-P-CAC, and KCM-P-WAC synthesized by the co-precipitation method are rather low. This indicates that the high-pressure impregnation method benefits the catalysts higher loading amounts of the copper manganese oxides. The contents of K in the four catalysts are almost at the same level.

N_2 adsorption–desorption tests

N_2 adsorption–desorption tests are performed to acquire the texture parameters. N_2 adsorption–desorption isotherms and pore size distributions of the catalysts are plotted in Figs. S2 and S3. According to the IUPAC (International Union of Pure and Applied Chemistry) classification, the isotherm of KCM-P-CSAC presents typical type-IV behavior with hysteresis loop of type H4, while those of KCM-P-CAC, KCM-P-WAC, and KCM-I-WAC reveal type-IV behavior with hysteresis loop of type H3. These indicate that the catalysts present the characteristics of mesoporous materials. The hysteresis loops located in the relative pressure range of

Table 1 Textural properties of the supports and catalysts

Samples	Surface area[a] (m^2/g)	Pore volume[b] (cm^3/g)	Average pore diameter[c] (nm)	Chemical compositions (wt%)		
				Cu	Mn	K
CSAC[d]	887.95	0.87	11.20	–	–	–
CAC[e]	734.95	0.62	3.41	–	–	–
WAC[f]	253.32	0.17	2.76	–	–	–
KCM-P-CSAC[g]	160.96	0.48	11.85	0.51	0.89	13.06
KCM-P-CAC[h]	79.57	0.09	4.61	0.43	0.96	12.31
KCM-P-WAC	67.67	0.08	4.89	0.23	0.58	11.82
KCM-I-WAC[i]	67.08	0.08	4.94	13.20	30.80	11.97

[a] Multi-point BET surface area

[b] Single point adsorption total pore volume at $P/P_0 = 0.97$

[c] Adsorption average pore width (4 V/A by BET)

[d] *CSAC* coconut-shell activated carbon

[e] *CAC* coal activated carbon

[f] *WAC* wood activated carbon

[g] *KCM* KOH modified copper manganese oxides

[h] *P* co-precipitation method

[i] *I* high-pressure impregnation method

0.45–0.99 are associated with the capillary condensation of nitrogen molecules in mesopores. It should be noticed that KCM-P-CSAC shows higher N_2 adsorption quantity, indicating that the catalyst owns better texture property.

Pore size distributions of the catalysts are displayed in Fig. S3. Most pores of KCM-P-CAC, KCM-P-WAC, and KCM-I-WAC are located in the pore diameter range of 2–10 nm. By contrast, KCM-P-CSAC shows a broader pore size distribution with pore diameter ranging from 2 to 100 nm. This should indicate a greater total volume for KCM-P-CSAC, compared to the other three catalysts.

Texture parameters including the BET surface areas, pore volumes and average pore diameters of the catalysts are listed in Table 1. For the sake of comparison, texture parameters of the supports are also provided. The BET surface areas of CSAC, CAC, and WAC are 887.95, 734.95 and 253.32 m^2/g. Their total pore volumes are calculated as 0.87, 0.62 and 0.17 cm^3/g. Both the surface areas and pore volumes show significant decrease after the loading of the active components. The surface areas of the four supported catalysts are 160.96, 79.57, 67.67 and 67.08 m^2/g. Their total pore volumes are determined as 0.48, 0.09, 0.08 and 0.08 cm^3/g. The loading of the active components over the supports has reduced the number of the active sites available for adsorption and caused pore blockage. The average pore diameters of the supports slightly increase, due to the reduction in their micropore volumes by the filling of the active components.

XRD analysis

The crystallinity and phase of the as-synthesized catalysts are determined by the XRD patterns, as shown in Fig. 1. The XRD profiles of the four catalysts show resembling diffraction peaks which could be assigned as CuO, $CuMn_2O_4$, Mn_2O_3, and KOH. The XRD spectra of KCM-P-CSAC, KCM-P-CAC, and KCM-P-WAC show another three peaks of high intensity, which should be attributed to SiO_2, $CaCO_3$, and Al_2O_3 in the supports. In contrast, these phases are not detectable in the profile of KCM-I-WAC. This should be ascribed to the fact that the high-pressure impregnation method has resulted in more uniform dispersion of copper manganese oxides over the support. As indicated in Table 1, the contents of Cu and Mn species in KCM-P-CSAC, KCM-P-CAC, and KCM-P-WAC are rather low. However, the XRD spectra of these catalysts show obvious diffraction peaks of high intensity for bulk CuO and Mn_2O_3, implying a weak interaction between the supports and the active components. The diffraction peaks for bulk CuO and Mn_2O_3 in the profile of KCM-I-WAC show lower intensity, despite the fact that the contents of Cu and Mn are high. This indicates that the active components of CuO and Mn_2O_3 are highly dispersed over the support for KCM-I-WAC.

FESEM analysis

Active components in the catalysts are generally utilized in the dispersed state, and the distribution characteristics of the active components over the supports affect their catalytic performances. To observe the dispersion characteristics of the active components, particle morphologies of the catalysts are examined, and the FESEM images are presented in Fig. 2.

Fig. 2 shows that many small grey blocks and white aggregates are dispersed on the surface of the catalysts. They are deduced as copper manganese oxides and KOH. For the morphology of KCM-P-CSAC, most of the active components are coated on the surface, channel wall, and grooves of the support. Although the

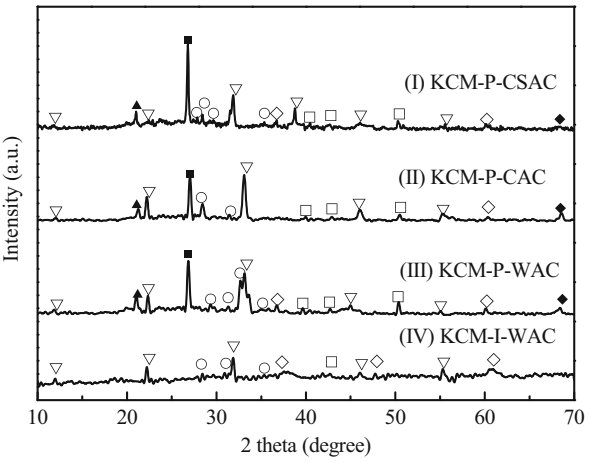

Fig. 1 XRD patterns of the catalysts. *Square*-CuO *Circle*-$CuMn_2O_4$ *Diamond*-Mn_2O_3 *Filled triangle*-SiO_2 *Filled square*-$CaCO_3$ *Filled diamond*-Al_2O_3 *Triangle*-KOH

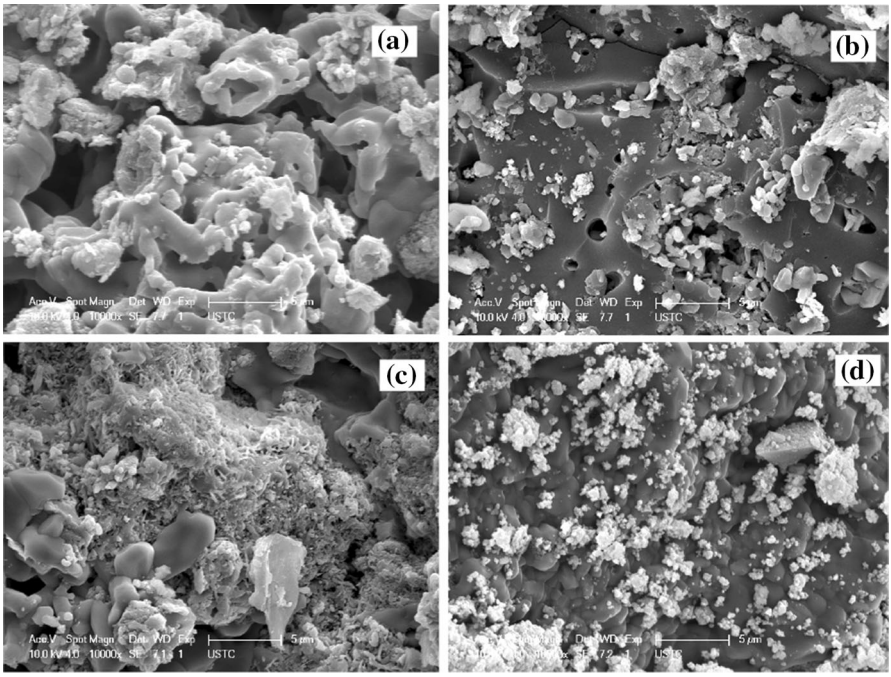

Fig. 2 FESEM images of the catalysts. **a** KCM-P-CSAC; **b** KCM-P-CAC; **c** KCM-P-WAC; **d** KCM-I-WAC

catalyst remains considerable pore structures that may contribute to the CO oxidation process, the active components are distributed unevenly with rather larger size. Particle morphology of KCM-P-CAC shows even surface, and the active components are uniformly distributed thereon. Although the micropores have been filled with the active components, the mesoporous structures are partially well remained, which are conducive to the gas diffusion and the contact with active components. It can be observed from the FESEM image of KCM-P-WAC that the loaded KOH aggregate as large white blocks and copper manganese oxides with large size scatter non-uniformly on the surface. These have induced the blockage of pore structures. Particle morphology of KCM-I-WAC shows that large quantities of copper manganese oxides granules combine with each other to form a plate-shaped precursor, and then the small white KOH aggregates are scattered over the precursor. Although the active components show more uniform distribution over the supports, their loadings have caused significant pore blockage.

FT-IR analysis

The as-synthesized catalysts are further characterized by FT-IR, and the spectra are presented in Fig. 3. The spectra of the catalysts exhibit IR bands at 510, 570, 700, 1400, and 3550 cm^{-1}. The characteristic absorption peak of CuO is reported to be located around 500 cm^{-1} [31]. The IR band at 510 cm^{-1} is thus deduced as the

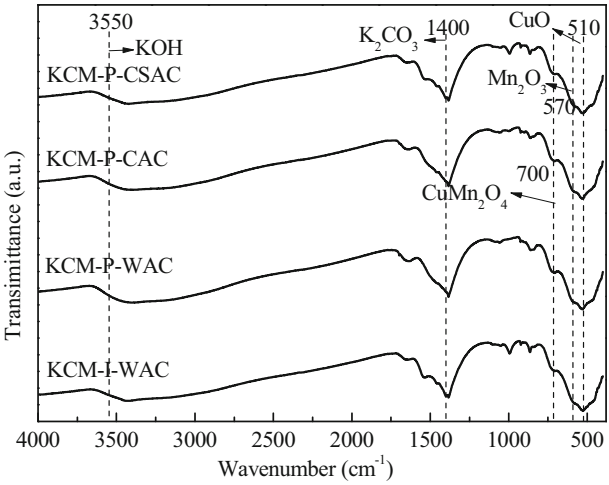

Fig. 3 FTIR spectra of the catalysts

vibrational feature of CuO. The weak IR band observed at 570 cm^{-1} could be attributed to Mn_2O_3. It is reported that compounds with spinel structure (AB_2O_4) would show broad absorption band in wavenumber range of 400–700 cm^{-1} due to the vibration of B^{3+}–O bond [32]. The absorption band observed at 700 cm^{-1} would correspond to the particular bond of $CuMn_2O_4$ phase. The significant absorption peak located around 1415 cm^{-1} is assigned as the symmetric stretching vibration of carbonate ions. The presence of carbonate ions could be deduced as the formation of K_2CO_3 via the carbonation reaction of KOH with CO_2 in open air atmosphere. The stretch vibrational frequency of hydroxyl ions in alkaline hydroxide is reported in the wavenumber range of 3550–3720 cm^{-1}. The IR band located at 3550 cm^{-1} can thus be assigned as KOH.

Catalytic activity

CO oxidation activities of the precursors and catalysts are tested in 0.4 %CO + 1.0 %CO_2 with balanced air, and the results are shown in Fig. 4. As indicated in Fig. 4a, CO conversions of CM-P-CSAC, CM-P-CAC, and CM-P-WAC increase slowly with the increasing temperature, whereas that of CM-I-WAC shows rapid increase. CM-I-WAC achieves its total CO conversion before the temperature reaches 200 °C. By contrast, CO conversions of CM-P-CSAC, CM-P-CAC, and CM-P-WAC are less than 50 % at 200 °C. These indicate that CM-I-WAC exhibits relatively higher CO oxidation activity.

Fig. 4b depicts that CO conversions of the catalysts versus temperature show similar variation with those of the precursors. Compared to the precursors, CO conversions of the catalysts are relatively higher. This indicated that CO oxidation activities of the precursors have been improved with the modification of KOH. It has been reported that KOH modification possesses a double functionality, namely, to mitigate the adverse effect of CO_2 by reducing its concentration driving force,

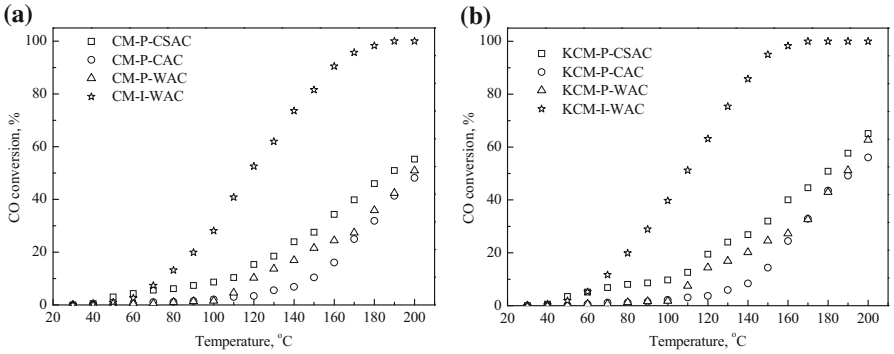

Fig. 4 CO oxidation activities of the precursors (**a**) and catalysts (**b**) tested in 0.4 %CO + 1.0 %CO_2 and balanced air

and to provide more oxygen adsorption sites to replenish the depleted oxygen in the CO oxidation process [33]. The temperature required for half CO conversion (T_{50}) must be focused on, since it is an important parameter for evaluating the catalytic activity. T_{50} values for KCM-P-CSAC, KCM-P-CAC, KCM-P-WAC, and KCM-I-WAC are 178, 190, 188 and 110 °C. The CO oxidation process should be more economically promising when operated at lower temperatures. Amongst the four catalysts, KCM-I-WAC exhibits the best catalytic activity toward CO oxidation with the lowermost T_{50} value.

Catalytic behaviors of the as-synthesized catalysts under different reaction conditions

Effect of support and synthesis method

CO oxidation activities of the catalysts prepared with different supports and methods have been elucidated in Fig. 4. To investigate the effect of support and synthesis method on their long-term working stabilities, CO conversions as a function of the time-on-stream are presented in Fig. 5.

As depicted in Fig. 5, when the final temperature is maintained at 200 °C, CO conversions of the four catalysts keep stable first and then decrease slightly. Within 90 min, CO conversions of KCM-P-CSAC, KCM-P-CAC, and KCM-P-WAC slightly decrease from 72.0, 65.7 and 68.8 % to 66.8, 63.7 and 61.3 %. KCM-I-WAC maintains its total CO conversion for 118 min, and its conversion slightly decreases to 95.9 % within 150 min. This indicates that KCM-I-WAC exhibits better long-term working stability for CO oxidation.

The difference in the CO oxidation activities amongst these catalysts could be ascribed to the texture properties of the supports and the coupling behaviors of the active components with the supports, due to the nature of the different activated carbons and the catalyst synthesis methods. Although KCM-P-CSAC exhibits better texture properties with higher surface area and greater pore volume, the active components are not uniformly dispersed and the utilization efficiency for the active

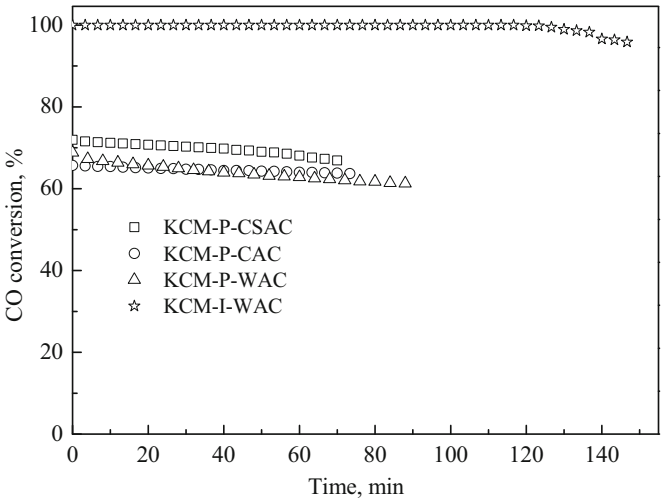

Fig. 5 Effect of support and synthesis method on long-term working stability (CO concentration: 0.4 %, CO_2 concentration: 1.0 %, air: balanced, GHSV: 4000 h^{-1}, particle size: 100 μm)

sites is rather low. For KCM-P-CAC and KCM-P-WAC, the loading of the active components has resulted in pore structure blockage and non-uniform dispersion of the active components on the supports. These could be possible reasons for the poor CO oxidation activities of KCM-P-CSAC, KCM-P-CAC, and KCM-P-WAC. Another major reason could be that the loading amounts of copper manganese oxides over the catalysts synthesized by the co-precipitation method are rather low. For KCM-I-WAC, although most of the pore structures have been destroyed by the loading of the active components, the high-pressure impregnation method has benefited the catalyst more uniform dispersion of the active components. This means that more active sites are readily available for the CO adsorption and catalytic oxidation process. Moreover, the high-pressure impregnation method could be favorable for the effective loading of copper manganese oxides. Therefore, these could be responsible for the preferable CO catalytic activity of KCM-I-WAC. Compared to the nature of the different activated carbon supports, catalyst synthesis method has exerted more significant impact on the CO oxidation activity.

Effect of CO concentration

The aforementioned analysis indicates that KCM-I-WAC exhibits the best CO oxidation activity in the presence of CO_2. Therefore, KCM-I-WAC is determined as a candidate to further investigate the effects of CO concentration, CO_2 concentration, GHSV, and particle size on CO oxidation activity. To investigate the effect of CO concentration, KCM-I-WAC is tested in CO + 1.0 %CO_2 and balanced air, whereby the CO concentration changes in the range of 0.1–0.5 %.

As shown in Fig. 6, the CO conversion of the catalyst decreases with the increase of CO concentration from 0.1 to 0.5 %. As shown in Table S1, T_{50} and T_{100} increase

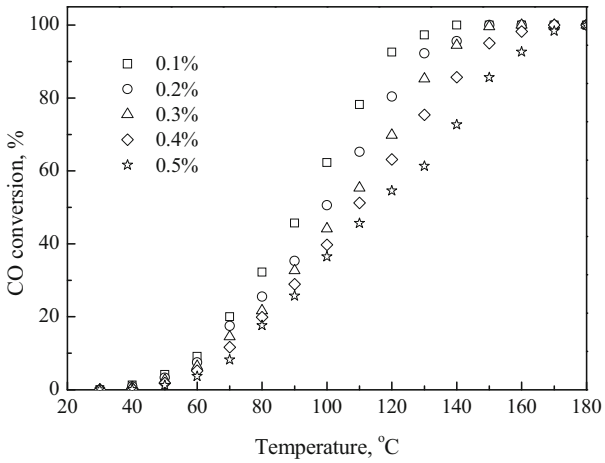

Fig. 6 Effect of CO concentration on CO oxidation activity. (Catalyst: KCM-I-WAC, CO concentration: 0.1–0.5 %, CO_2 concentration: 1.0 %, air: balanced, GHSV: 4000 h^{-1}, particle size: 100 μm)

from 93.1 and 140 °C to 115.8 and 180 °C, when the CO concentration increases from 0.1 to 0.5 %. CO conversions of the catalyst in different CO concentrations are correlated with the reaction rate, as shown in Fig. S4. CO oxidation reaction rate increases first and then keeps stable with the increasing reaction temperature. With the increase of CO concentration from 0.1 to 0.5 %, the CO oxidation reaction rate increases from 0.89×10^{-7} to 2.03×10^{-7} mol g^{-1} s^{-1}, when the catalyst is tested at 120 °C. Luo et al. reported that, with the increasing CO partial pressure from 0.3040 to 3.0398 kPa, CO conversion of Pt/TiO_2 decreased from 17.4 to 3.6 %, and its reaction rate increased from 1.55×10^{-7} to 3.21×10^{-7} mol g^{-1} s^{-1}, when the catalyst was tested at 40 °C [34]. On the one hand, the increase in CO concentration enhances the CO concentration driving force, and benefit the catalyst increased reaction rate. On the other hand, more CO_2 is generated under higher CO partial pressures, and they compete with CO for the adsorption active sites to form surface carbonate species, and therefore to inhibit the CO oxidation process by reducing the CO conversion [35].

Effect of CO_2 concentration

It has been confirmed that CO_2 would exert adverse effect the oxidation activities of CO catalysts. To investigate the effect of CO_2, KCM-I-WAC is tested in 0.4 %CO + CO_2 and balanced air, whereby the CO_2 concentration varies from 0.5 to 15.0 %.

As shown in Fig. 7, CO conversion of the catalyst decreases with the increasing CO_2 concentration from 0.5 to 15.0 %. T_{50} and T_{100} increase from 105.9 and 160 °C to 142.1 and 200 °C when the CO_2 concentration increases from 0.5 to 15.0 %. CO oxidation activity could hardly be affected when the catalyst is tested under lower CO_2 concentrations of 0.5 and 1.0 %. Nevertheless, CO conversion shows

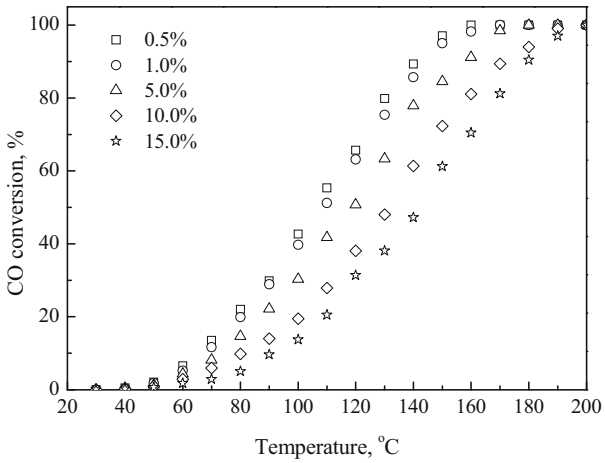

Fig. 7 Effect of CO_2 concentration on CO oxidation activity. (Catalyst: KCM-I-WAC, CO concentration: 0.4 %, CO_2 concentration: 0.5–15.0 %, air: balanced, GHSV: 4000 h^{-1}, particle size: 100 μm)

significant decrease when the CO_2 concentration further increases in the range of 5.0–15.0 %. The presence of CO_2 competes with CO and O_2 to take up the adsorption active sites and therefore inhibit the CO adsorption process [36, 37]. KOH modification can effectively mitigate the adverse effect of CO_2 under lower CO partial pressures. When the CO_2 partial pressure increases to a high value, more bicarbonate species are formed. The generated bicarbonate species cover the surface active sites and cause pore blockage, and therefore impair the CO oxidation process.

Effect of GHSV

To study the effect of GHSV on CO oxidation activity, KCM-I-WAC is tested in 0.4 %CO + 1.0 %CO_2 and balanced air, whereby the GHSV changes from 2400 to 5600 h^{-1}.

Fig. 8 shows that CO conversion of the catalyst decreases with the increase of GHSV. With the increase of GHSV from 2400 to 5600 h^{-1}, T_{50} and T_{100} increase from 103.4 and 170 °C to 125.4 and 180 °C. The effect of GHSV on CO oxidation reaction rate is also presented in Fig. S5. With the increase of GHSV from 2400 to 5600 h^{-1}, CO oxidation reaction rate increases from 1.24×10^{-7} to 2.10×10^{-7} mol g^{-1} s^{-1}, when the catalyst is tested at 120 °C. The increase in GHSV means that more reactants are replenished to the CO catalytic reaction. Besides, the increasing GHSV would be conducive to decreasing the thickness of the boundary layer and benefits the catalyst facilitative mass-transfer process. These improve the CO oxidation reaction rate. In contrast, the increasing GHSV also indicates reduced reaction residence time and therefore the overall CO conversion is decreased. These are in line with the results reported in previous publications [35, 37–39].

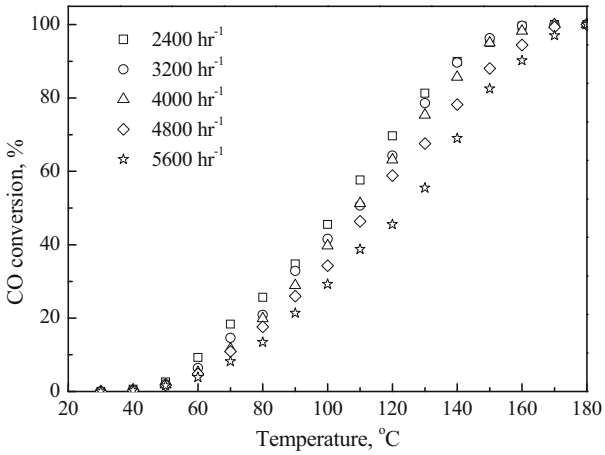

Fig. 8 Effect of GHSV on CO oxidation activity. (Catalyst: KCM-I-WAC, CO concentration: 0.4 %, CO_2 concentration: 1.0 %, air: balanced, GHSV: 2400–5600 h^{-1}, particle size: 100 μm)

Effect of particle size

Particle size is an important factor affecting the activities of heterogeneous catalysts [40]. To study the particle size effect, the catalysts with particle diameter ranging from 60 to 300 μm are tested in 0.4 %CO + 1.0 %CO_2 and balanced air.

Fig. 9 depicts that the CO conversion of KCM-I-WAC decreases with the increase of particle diameter. With the increasing particle diameter from 60 to 300 μm, T_{50} and T_{100} increase from 108.6 and 170 °C to 157.8 and 200 °C. Internal diffusion is one significant parameter that affect the CO oxidation activity. The

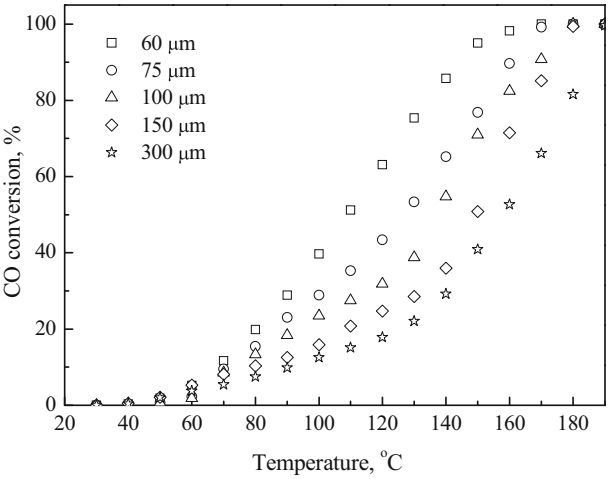

Fig. 9 Effect of particle size on CO oxidation activity. (Catalyst: KCM-I-WAC, CO concentration: 0.4 %, CO_2 concentration: 1.0 %, air: balanced, GHSV: 4000 h^{-1}, particle size: 60–300 μm)

internal diffusion effect is characterized by the intra-particle diffusion efficiency factor η, which is defined as the ratio of the real reaction rate affected by internal diffusion to that of the limit reaction rate free from the influence of internal diffusion [41]. A greater value for η should indicate non-significant impact of internal diffusion on CO oxidation activity. Meanwhile, the Thiele modulus φ_s is the only influential factor for η:

$$\eta = \frac{1}{\varphi_s}\left[\frac{1}{th(3\varphi_s)} - \frac{1}{3\varphi_s}\right]$$

For the first order CO catalytic reaction, φ_s could be correlated with the particle diameter:

$$\varphi_s = \frac{R}{3}\sqrt{\frac{k}{D_e}}$$

Here R is the particle diameter, k is the kinetic constant per volume, and D_e is the effective diffusion coefficient.

With the increase of particle diameter R, the Thiele modulus φ_s is increased, and the intra-particle diffusion efficiency factor η is decreased. This indicates that the intra-particle diffusion process exerts significant impact on the CO oxidation activity. Therefore, reducing the particle size of the catalyst could be the most effective means for reducing the intra-particle diffusional resistance. Therefore, to increase the CO oxidation activity and to decrease the internal diffusion resistance, the particle diameter of the catalyst should be controlled at a lower value in practical operations.

Conclusions

In this work, copper manganese oxides precursors with different activated carbon supports are synthesized using the co-precipitation and high-pressure impregnation methods. The precursors are further modified by KOH to synthesize the bi-functional catalysts with improved CO_2-resistance. The CO oxidation performances of the catalysts are evaluated in the presence of CO_2 using a fixed-bed reactor. The effects of the support, catalyst synthesis method and operating parameters on CO oxidation performances are demonstrated. Compared to the nature of the different activated carbons, the catalyst synthesis method exerts more significant effect on CO oxidation performances. Amongst all these catalysts, KCM-I-WAC synthesized by the high-pressure impregnation method with wood activated carbon as support exhibits excellent CO oxidation activity and long-term working stability. The high-pressure impregnation method benefits the catalyst effective loading and uniform dispersion of the active components. The CO conversion decreases with the increasing CO and CO_2 partial pressures, due to the covering of the adsorption active sites and the formation of surface carbonate/bicarbonate species. Increasing GHSV shortens the reaction residence time and therefore decrease the overall CO

conversion. The increase in particle diameter is detrimental to high CO conversion, due to the adverse effect of internal diffusion. The results provide insights into optimizing the synthesis method and operation parameters for enhanced CO oxidation performances. The bi-functional catalyst with high CO_2-resistance shows promise as a scavenger agent for post-fire atmosphere recovery application. Future work will be focused on evaluating CO oxidation performances of the catalyst in the atmosphere more close to a real post-fire smoke scenario, considering the impurities such as H_2O, NO_x, SO_x, HCl and HCN.

Acknowledgments Financial support from the National Natural Science Foundation of China (U1510129 and 51323010) and the Fundamental Research Funds for the Central Universities (WK2320000034) is sincerely acknowledged. The authors also wish to acknowledge Dr. Yanming Ding for the English editing for this article.

References

1. Karanjikar A (2005) Auburn University, Alabama. https://etd.auburn.edu/handle/10415/1276
2. Gold A, Burgess WA, Clougherty EV (1978) Am Ind Hyg Assoc J 39:534–539
3. Terrill JB, Montgomery RR, Reinhardt CF (1978) Science 200:1343–1347
4. Behar S, Gonzalez P, Agulhon P, Quignard F, Świerczyński D (2012) Catal Today 189:35–41
5. Krämer M, Schmidt T, Stöwe K, Maier WF (2006) Appl Catal A 302:257–263
6. Yoon C, Cocke DL (1988) J Catal 113:267–280
7. Hasegawa Y, Fukumoto K, Ishima T, Yamamoto H, Sano M, Miyake T (2009) Appl Catal B 89:420–424
8. Clarke TJ, Davies TE, Kondrat SA, Taylor SH (2015) Appl Catal B 165:222–231
9. Wojciechowska M, Przystajko W, Zieliński M (2007) Catal Today 119:338–341
10. Li M, Wang DH, Shi XC, Tang ZT, Dong TX (2007) Sep Purif Technol 57:147–151
11. Einaga H, Kiya A (2016) Reac Kinet Mech Cat 117:521–536
12. Jia AP, Deng Y, Hu GS, Luo MF, Lu JQ (2016) Reac Kinet Mech Cat 117:503–520
13. Choi KH, Lee DH, Kim HS, Yoon YC, Park CS, Kim YH (2016) Ind Eng Chem Res 55:4443–4450
14. Caputo T, Lisi L, Pirone R, Russo G (2007) Ind Eng Chem Res 46:6793–6800
15. Hasegawa YI, Maki RU, Sano M, Miyake T (2009) Appl Catal A 371:67–72
16. Njagi EC, Chen CH, Genuino H, Galindo H, Huang H, Suib SL (2010) Appl Catal B 99:103–110
17. Jones C, Cole KJ, Taylor SH, Crudace MJ, Hutchings GJ (2009) J Mol Catal A 305:121–124
18. Hutchings GJ, Mirzaei AA, Joyner RW, Siddiqui MRH, Taylor SH (1998) Appl Catal A 166:143–152
19. Ren N, Guo L, Dong X, Wen C (2015) Transit Metal Chem 40:207–216
20. Cao JL, Wang Y, Sun G, Zhang ZY (2011) Transit Metal Chem 36:107–112
21. Barbato PS, Benedetto AD, Landi G, Lisi L (2015) Chem Eng J 279:983–993
22. Li JJ, Li L, Cheng W, Wu F, Lu XF, Li ZP (2014) Chem Eng J 244:59–67
23. Liu XS, Jin ZN, Lu JQ, Wang XX, Luo MF (2010) Chem Eng J 162:151–157
24. Peng CT, Lia HK, Liaw BJ, Chen YZ (2011) Chem Eng J 172:452–458
25. Hoflund GB, Gardner SD, Schryer DR, Upchurch BT, Kielin EJ (1995) Langmuir 11:3431–3434
26. Liang F, Zhu H, Qin Z, Wang G, Wang J (2009) Catal Commun 10:737–740
27. Parinyaswan A, Pongstabodee S, Luengnaruemitchai A (2006) Int J Hydrogen Energy 31:1942–1949
28. Wang F, Zhao K, Zhang H, Dong Y, Wang T, He D (2014) Chem Eng J 242:10–18
29. Oudenhuijzen MK (2002) Utrecht University, Netherlands. http://dspace.library.uu.nl/handle/1874/761
30. De Mallmann A, Barthomeuf D (1990) J Chim Phys 87:535–538
31. Ethiraj AS, Kang DJ (2012) Nanoscale Res Lett 7:1–5
32. Valdés-Solís T, López I, Marbán G (2010) Int J Hydrogen Energy 35:1879–1887
33. Guo YF, Li CH, Lu SX, Zhao CW (2016) RSC Adv. 6:7181–7188
34. Li N, Chen QY, Luo LF, Huang WX, Luo MF, Hu GS, Lu JQ (2013) Appl Catal B 142–143:523–532

35. Shen Y, Lu G, Guo Y, Wang Y, Guo Y, Gong X (2011) Catal Today 175:558–567
36. Lou Y, Wang L, Zhao Z, Zhang Y, Zhang Z, Lu G, Guo Y (2014) Appl Catal B 146:43–49
37. Srivastava AK, Saxena A, Shah D, Mahato TH, Singh B, Shrivastava AR, Shinde CP (2012) J Hazard Mater 241–242:463–471
38. Wang L, Wang W, Zhang Y, Guo Y, Lu G, Guo Y (2015) Catal Today 242:315–321
39. Biabani-Ravandi A, Rezaei M (2012) Chem Eng J 184:141–146
40. Li N, Chen QY, Luo LF, Huang WX, Luo MF, Hu GS, Lu JQ (2013) Appl Catal B 142:523–532
41. Thomas JM, Thomas WJ (2014) Principles and practice of heterogeneous catalysis. Wiley, Germany